

Star Formation and Dust Extinction Properties of Local Galaxies as seen from AKARI and GALEX

A. Sakurai¹, T. T. Takeuchi¹, F.-T. Yuan¹, V. Buat², and D. Burgarella²

¹Division of Particle and Astrophysical Science, Nagoya University, Furo-cho, Chikusa-ku, Nagoya 464-8602, Japan

²Aix Marseille Université, CNRS, LAM (Laboratoire d'Astrophysique de Marseille) UMR 7326, 13388, Marseille, France

(Received xxxx xx, 2011; Revised xxxx xx, 2012; Accepted xxxx xx, 2012; Online published Xxxxx xx, 2008)

An accurate estimation of the star formation-related properties of galaxies is crucial for understanding the evolution of galaxies. In galaxies, ultraviolet (UV) light emitted by recently formed massive stars is attenuated by dust, which is also produced by star formation (SF) activity, and is reemitted at mid- and far- infrared (IR) wavelengths. In this study, we investigate the star formation rate (SFR) and dust extinction using UV and IR data. We selected local galaxies which are detected at AKARI FIS 90 μm and matched the IRAS IIFSCz 60 μm select catalog. We measured FUV and NUV flux densities from GALEX images. We examined the SF and extinction of Local galaxies using four bands of AKARI. Then, we calculated FUV and total IR luminosities, and obtained the SF luminosity, L_{SF} , the total luminosity related to star formation activity, and the SFR. We find that in most galaxies, L_{SF} is dominated by L_{dust} . We also find that galaxies with higher SF activity have a higher fraction of their SF hidden by dust. In fact, the SF of galaxies with SFRs $> 20 \text{ M}_{\odot} \text{ yr}^{-1}$ is almost completely hidden by dust. Our results boast a significantly higher precision with respect to previously published works, due to the use of much larger object samples from the AKARI and GALEX all sky surveys.

Key words: Dust; galaxies: formation; galaxies: evolution; stars: formation; infrared; ultraviolet.

1. Introduction

The evolution of galaxies is one of the most fundamental problems in modern observational cosmology. Since all heavy elements (elements whose atomic number is larger than Boron) have not been produced by Big Bang Nucleosynthesis but rather by stars, the investigation of star formation is related to the quest for the comprehending the origin of the Earth, planets, and ourselves.

An accurate estimation of the star formation-related properties of galaxies is crucial for the understanding of the evolution of galaxies. The total mass of newly formed stars in a galaxy per year is referred to as the star formation rate (SFR) (Takeuchi et al., 2010). Massive stars are known to be good indicators of star formation (SF) activity, since they have much shorter lifetime ($\sim 10^{6-8} \text{ yr}$) than the age of galaxies and the Universe ($\sim 10^{10} \text{ yr}$) and therefore are regarded as an “instantaneous” indicator of the SFR in galaxies.

Massive stars (OB stars) are hot and emit ultraviolet light. The UV spectra is dominated by emission from massive stars. Then, we can *in principle* obtain the SFR of galaxies directly by measuring their UV luminosity. However, as mentioned above, stars produce heavy elements (or metals¹) and release them through explosive phenomena during the final phases of stellar evolution such as planetary nebulae, supernova explosions, and some other mass ejection processes (e.g., Asano et al., 2012).

A significant fraction of metals are in the form of tiny solid grain (the typical size is smaller than $1 \mu\text{m}$) in the ISM, referred to as dust (Mathis, 1990). This means that SF activity in galaxies is always accompanied by dust formation, except for the formation of the very first stars in the Universe, and the dust grains are gradually mixed with the ISM. The UV photons from massive stars are easily absorbed and/or scattered by dust grains and re-emitted as mid- and far-infrared photons. This is referred to as dust extinction. We stress here that if we only measure the UV photons from massive stars in galaxies, SF activity can be seriously underestimated because a significant amount of the energy is obscured by dust (e.g., Kennicutt, 1998). Indeed, Takeuchi et al. (2005a) have shown that a significant amount of the cosmic SFR density is obscured by dust and can only be observed through far-IR radiation. They found that the fraction of hidden SF increases from 50–60% at $z = 0$ to $> 90\%$ at $z = 1$. This finding was confirmed and further explored by recent studies (e.g., Murphy et al., 2011; Cucciati et al., 2012).

Many attempts have been made to explore star formation in UV and IR to have an unbiased view of star formation in the Universe (e.g., Seibert et al., 2005; Martin et al., 2005; Cortese et al., 2006; Buat et al., 2007; Lee et al., 2009; Noll et al., 2009; Haines et al., 2011; Bothwell et al., 2011).

In order to estimate the SFR of galaxies accurately, it is ideal to combine UV-related observables and dust-related ones. Recently various methods on this matter have been proposed (e.g., Iglesias-Páramo et al., 2006; Kennicutt et al., 2009; Calzetti et al., 2010; Hao et al., 2011, among others). In this study, we adopt the simplest SFR estimator: a combination of SFRs estimated from UV and FIR continuum radiation (Iglesias-Páramo et al., 2006). To this aim we con-

Copy right© The Society of Geomagnetism and Earth, Planetary and Space Sciences (SGEPSS); The Seismological Society of Japan; The Volcanological Society of Japan; The Geodetic Society of Japan; The Japanese Society for Planetary Sciences; TERRAPUB.

¹ A terminology indicating elements heavier than helium.

structed a new dataset from GALEX (UV) and AKARI (IR) observations. Thanks to these two all-sky surveyor satellites, we have one database which contains an unprecedented amount of UV-IR data of Local galaxies. Making use of this new database, we explore the SF- and extinction-related properties of galaxies in the Local Universe in a similar manner to a previous work of Takeuchi *et al.* (2010) which used the beta version of AKARI data.

This paper is organized as follows: in Section 2, we introduce the AKARI and GALEX data and explain the construction of the infrared-selected IR-UV dataset. In Section 3 we describe the basic results of this study, and in Section 4 we interpret the UV and IR properties of our sample galaxies. Section 5 is dedicated to our summary and conclusion.

Throughout this paper we will assume $\Omega_{M0} = 0.3$, $\Omega_{\Lambda0} = 0.7$ and $H_0 = 70 \text{ km s}^{-1} \text{ Mpc}^{-1}$. The luminosities are defined as νL_ν and expressed in solar units assuming $L_\odot = 3.83 \times 10^{33} \text{ erg s}^{-1}$.

2. Data

2.1 AKARI

AKARI was launched by JAXA (Japan Aerospace eXploration Agency) in February 2006 (Murakami *et al.*, 2007)². AKARI was equipped with two imaging instruments, the Far-infrared Surveyor (FIS: Kawada *et al.*, 2007) and the Infrared Camera (IRC: Onaka *et al.*, 2007), together with a Fourier spectrograph (FTS: Kawada *et al.*, 2008).

Before AKARI, the Infrared Astronomical Satellite, IRAS, performed the first all-sky survey at mid- and far-IR (MIR and FIR) wavelengths. The IRAS all-sky survey has yielded a vast amount of statistics for dusty galaxies in the Local Universe. The survey provided a point source catalog (IRAS PSC) and has long been used for extragalactic studies (see e.g., Soifer *et al.*, 1987). IRAS covered mid- and far-IR wavelength bands: 12 μm , 25 μm , 60 μm , and 100 μm . Though the IRAS PSC has made a revolutionary impact on the studies of IR objects, the lack of wavebands at $\lambda > 100 \mu\text{m}$ restricted the range of application to dusty object studies.

This is one of the reasons why AKARI was designed to perform an IR all sky survey, especially at wavelengths longer than 100 μm . The AKARI FIS All-Sky Survey was carried out with four photometric wavebands at FIR, centered at 65 μm (*N60*), 90 μm (*WIDE-S*), 140 μm (*WIDE-L*), and 160 μm (*NI60*), with a better sensitivity and angular resolution than that of IRAS. The point source catalogs and diffuse maps have been gradually made public to the astronomical community.

2.2 GALEX

The UV satellite GALEX (Galaxy Evolution Explorer) was launched by NASA (the National Aeronautics and Space Administration) as one of the SMEX (Small Explorer program) missions in April 2003³. GALEX has two photometric bands, FUV (1350-1750 \AA , $\lambda_{\text{mean}} = 1530 \text{ \AA}$) and NUV (1750-2750 \AA , $\lambda_{\text{mean}} = 2310 \text{ \AA}$). GALEX data products include a series of all sky surveys and deep sky sur-

veys in the imaging mode and partial surveys in the NUV and FUV spectroscopic modes. In this study we use the data of GALEX releases GR4/GR5 all sky imaging survey (AIS) with detection limits of 19.9 mag and 20.8 mag in AB system (Morrissey *et al.*, 2007).

2.3 Sample construction

2.3.1 Matching AKARI BSC with IRAS IIFSCz As a basis for the construction of our galaxy sample we used the AKARI FIS bright source catalog (BSC) v.1 from the AKARI all sky survey (Yamamura *et al.*, 2010). The sources in the AKARI FIS BSC v. 1 have a three times better S/N ratio than the previous catalog, AKARI FIS BSC β -1 (Yamamura *et al.*, 2008), which was used by Takeuchi *et al.* (2010). This provides various advantages for the analysis of this work. Since AKARI BSC sources contain all kinds of IR objects, like AGBs, Vega-like stars, HII regions, planetary nebulae, etc. (Pollo *et al.*, 2010), the first step of this study is to construct a catalog of galaxies. In order to have a secure sample of galaxies with redshift data, we made a cross match of AKARI sources with the Imperial IRAS-FSC Redshift Catalogue (IIFSCz), a redshift catalog recently published by Wang and Rowan-Robinson (2009). The IIFSCz is based on the IRAS Faint Source Catalog (FSC). In the IRAS FSC, the flux density quality (FQUAL) is classified as high (= 3), moderate (= 2) or upper limit (= 1). The IIFSCz has FQUAL = 3 and a signal-to-noise ratio > 5 at 60 μm . Wang and Rowan-Robinson (2009) selected galaxy candidates by using the following color (flux ratio) conditions: (i) $\log(S_{100}/S_{60}) < 0.8$ (if FQUAL ≥ 2 at 100 μm), (ii) $\log(S_{60}/S_{12}) > 0$ (if FQUAL ≥ 2 at 12 μm)⁴. This catalog contains 60,303 galaxies, and 90 % of them have spectroscopic or photometric redshifts at $S_{60} > 0.36 \text{ Jy}$. In this sample, we put a limit on the recession velocity of $v > 1000 \text{ km s}^{-1}$, in order to avoid the effect of the peculiar velocities of galaxies. Then, we matched the AKARI BSC sources with these IIFSCz galaxies using a search radius of 36 arcsec, which corresponds to the position uncertainty of the IRAS catalog. If there are multiple counterpart candidates in the search radius, the closest one is chosen. After concluding all of the steps described above we obtained 6674 IR galaxies and used them for the GALEX photometry.

2.3.2 GALEX photometry We measured FUV and NUV flux densities for the 6674 galaxies from GALEX images by using a software package developed specially for this purpose. Details of this package are explained in Iglesias-Páramo *et al.* (2006).

We performed the UV photometry as follows:

- 1) Cut out a $20' \times 20'$ subimage from GALEX GR4/GR5 images around each AKARI galaxy.
- 2) Select the subimage with the largest exposure time.
- 3) Measure the FUV and NUV flux densities from the imagelet.
 - (a) Define the center, major axis, and minor axis to fit the ellipse using the NUV subimages and apply the fitted regions to FUV subimages.

² URL: <http://www.ir.isas.ac.jp/ASTRO-F/index-e.html>.

³ URL: <http://www.galex.caltech.edu/>.

Here we used the convention of IRAS flux densities: $S_{\text{IRAS band}} \equiv S_\nu / \text{IRAS band [Jy]}$.

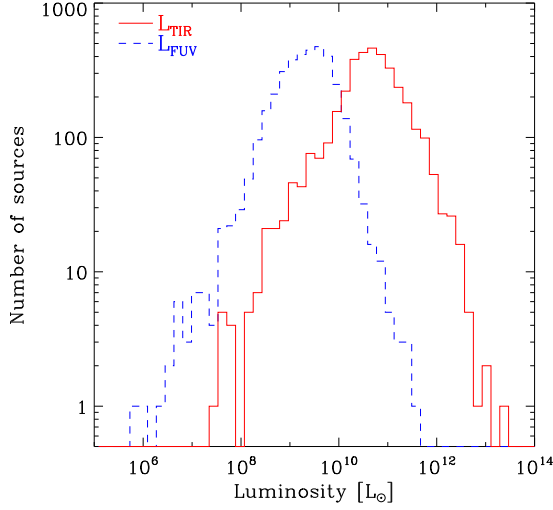


Fig. 1. L_{TIR} and L_{FUV} distributions of our sample. Dashed and solid histograms represent the distributions of L_{FUV} and L_{TIR} , respectively.

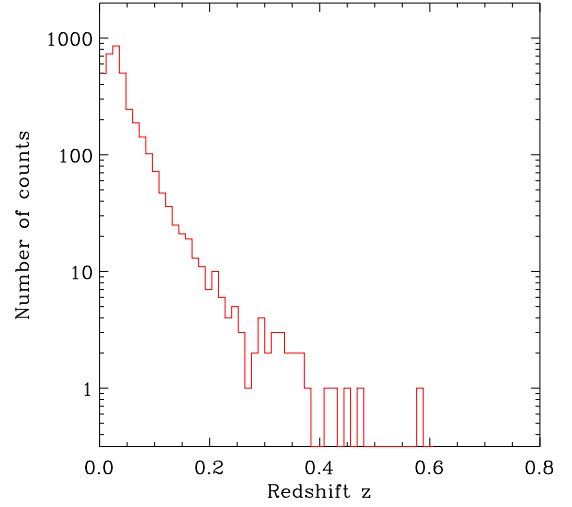


Fig. 2. Redshift distribution of the sample galaxies. Redshift data are taken from the Imperial IRAS FSC Redshift Catalog (IIFSCz) (Wang and Rowan-Robinson, 2009).

- (b) Define the sky background level around the major axis.
- (c) Expand the ellipsoidal measured range without changing the axis ratio from the center.
- (d) Stop to measure when the flux density does not change more than the background.

The FUV and NUV flux densities are corrected for Galactic extinction by extracting the $E(B - V)$ values from the Schlegel Map (Schlegel et al., 1998) and assuming the Galactic extinction curve calculated by Cardelli et al. (1989).

IR objects which did not have a counterpart in FUV and NUV were excluded from further analysis. The images which contain stars in the considered region or partial galaxies (due to the GALEX image limit), were also left out from subsequent research. This process reduced the number of selected galaxies in the parent sample to 3981. Among them, there are galaxies which have flux densities below the detection limits of GALEX AIS at NUV and/or FUV. In such a case, we replaced these unreliable values with the flux density detection limits. Therefore, the effective number of galaxies which satisfied the completeness criteria was reduced to 3567, and these were used for our analysis.

3. Basic Results

3.1 Luminosity of galaxies

First of all, we calculated the luminosity of sample galaxies from their measured flux density. The flux density S_ν at a frequency ν and the monochromatic luminosity L_ν (the luminosity per frequency) of an object are related through the following equation:

$$L_\nu d\nu = 4\pi d_L^2(z) S_\nu d\nu, \quad (1)$$

where $d_L(z)$ is the luminosity distance of an object at redshift z . Given the Hubble parameter $H(z)$ at redshift z and the velocity of light c , $d_L(z)$ is expressed as

$$d_L(z) = (1+z) \int_0^z \frac{c}{H(z')} dz' \quad (2)$$

where

$$H(z) = H_0 \left[\Omega_{\text{M}0}(1+z)^3 - (\Omega_{\text{M}0} + \Omega_{\Lambda 0} - 1)(1+z)^2 + \Omega_{\Lambda 0} \right]^{\frac{1}{2}}. \quad (3)$$

Then we obtain,

$$\begin{aligned} L_{\nu_{\text{em}}} d\nu_{\text{em}} &= L_{(1+z)\nu_{\text{obs}}} (1+z) d\nu_{\text{obs}} \\ &= \frac{4\pi d_L^2 S_{\nu_{\text{obs}}}}{1+z} (1+z) d\nu_{\text{obs}} \\ &= 4\pi d_L^2 d\nu_{\text{obs}} S_{\nu_{\text{obs}}}, \end{aligned} \quad (4)$$

where

$$\nu_{\text{obs}} = \frac{\nu_{\text{em}}}{1+z}. \quad (5)$$

The AKARI- and GALEX-band luminosities are calculated with the following formulae because of the different definitions of AKARI and GALEX photometry.

$$\begin{aligned} L_{\text{AKARI band}} &\equiv \Delta\nu L_\nu \\ &= \Delta\nu(\text{AKARI band}) 4\pi d_L^2 S_{\nu(@\text{AKARI band})}, \end{aligned} \quad (6)$$

$$\begin{aligned} L_{\text{GALEX band}} &\equiv \nu L_\nu \\ &= \nu(@\text{GALEX band}) 4\pi d_L^2 S_{\nu(@\text{GALEX band})}. \end{aligned} \quad (7)$$

Here, $\Delta\nu(\text{AKARI band})$ stands for the frequency range of the AKARI bands, and $\nu(@\text{GALEX band})$ stands for the effective frequencies of the GALEX bands.

3.2 Total IR luminosity

We first obtained the total IR (TIR) luminosity L_{TIR} from AKARI FIS bands. Hirashita et al. (2008) proposed a formula to estimate the TIR luminosity at $\lambda = 3\text{--}1000 \mu\text{m}$ using the flux densities of three AKARI bands: *N60*, *WIDE-S*, and *WIDE-L*, for the AKARI pointed observation sample

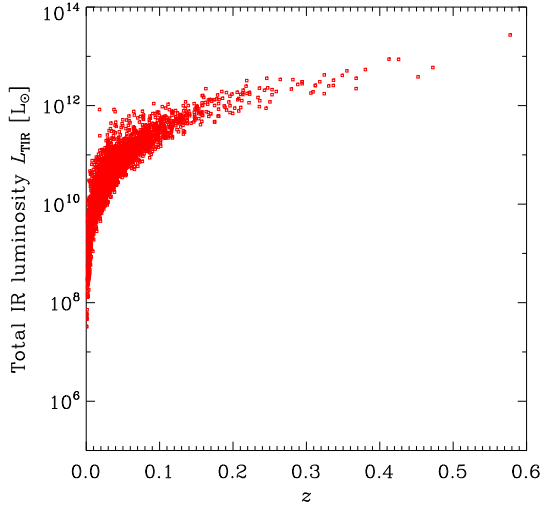
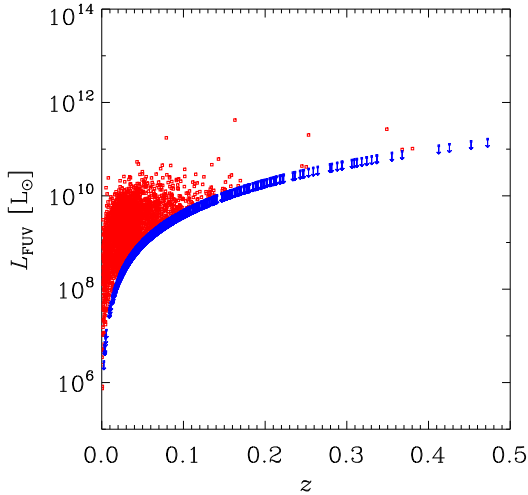


Fig. 3. The redshift-total IR (TIR) luminosity distribution.

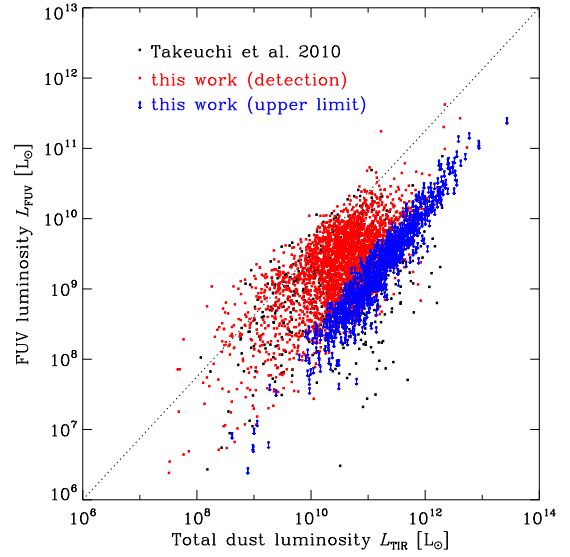
Fig. 4. The redshift-FUV luminosity relations. Open squares represent the FUV luminosities and the downward arrows show galaxies which have FUV flux densities below the detection limit of GALEX AIS. The FUV detection limit is 19.9 mag in AB system (Morrissey *et al.*, 2007).

of dwarf star-forming galaxies and blue compact galaxies. Their formula was examined and confirmed to be valid for the AKARI FIS All-Sky Survey galaxies by Takeuchi *et al.* (2010). However, since the flux density at $N60$ was noisier than in the wide bands, Takeuchi *et al.* (2010) found that an alternative formula which makes use of only *WIDE-S* and *WIDE-L* flux densities gives a tighter relation than that for three bands. Hence, in this study we adopted the formula of Takeuchi *et al.* (2010) to estimate TIR luminosity.

$$L_{\text{AKARI}}^{2\text{band}} = \Delta\nu(\text{WIDE-S})L_\nu(90 \mu\text{m}) + \Delta\nu(\text{WIDE-L})L_\nu(140 \mu\text{m}), \quad (8)$$

where

$$\begin{aligned} \Delta\nu(\text{WIDE-S}) &= 1.47 \times 10^{12} \text{ [Hz]} \\ \Delta\nu(\text{WIDE-L}) &= 0.831 \times 10^{12} \text{ [Hz]}. \end{aligned} \quad (9)$$

Fig. 5. Relation between L_{FUV} and L_{TIR} . The diagonal dotted line represents the case if L_{FUV} equals L_{TIR} . Black dots represent the data from Takeuchi *et al.* (2010). Downward arrows represent galaxies which have UV flux densities below the detection limit of GALEX.

The conversion formula from $L_{\text{AKARI}}^{2\text{band}}$ to L_{TIR} is

$$\log L_{\text{TIR}} = 0.964 \log L_{\text{AKARI}}^{2\text{band}} + 0.814 \quad (10)$$

The distributions of the FUV and TIR luminosities are shown in Fig. 1. We see that the two distributions are significantly different from each other. The first reason for the difference is that our sample is AKARI 90- μm and IRAS IIFSCz 60 μm selected, i.e., they are inclined to dustier galaxies. Then, the UV continuum of the sample galaxies is extinguished by dust, leading to lower luminosities in the NUV and FUV bands. Another reason is because of the well known difference in the shape of the luminosity function between UV and IR (Buat & Burgarella, 1998; Takeuchi *et al.*, 2005a), especially at the highest luminosities. The peak luminosities at FUV and TIR are also significantly different. More detailed analysis on the luminosity functions at UV and IR is presented in (Takeuchi *et al.*, 2012b).

3.3 Redshift and luminosity distributions

The redshift distribution of our sample is shown in Fig. 2. We see that most of the sample galaxies are at low redshifts of $z \lesssim 0.5$. The peak of the redshift distribution is located at $z \simeq 0.02$, almost the same as that of the IIFSCz.

Figure 3 shows the redshift-TIR luminosity distribution. The selection boundary due to the flux detection limit is clearly seen. In statistical terminology this case is referred to “truncated” meaning that we cannot know if there would be objects below the detection limit.

We show the relation between the redshift and FUV luminosity in Fig. 4. The small squares represent the detection at FUV, while the downward arrows show the upper limits of the luminosities. Due to the fact that our sample is primarily selected at 90 μm (see Fig. 3) some galaxies detected in IR will be invisible at UV bands (see Fig. 4). This case is referred to as “censored”. This difference is important when we try to estimate a luminosity function. We discuss this

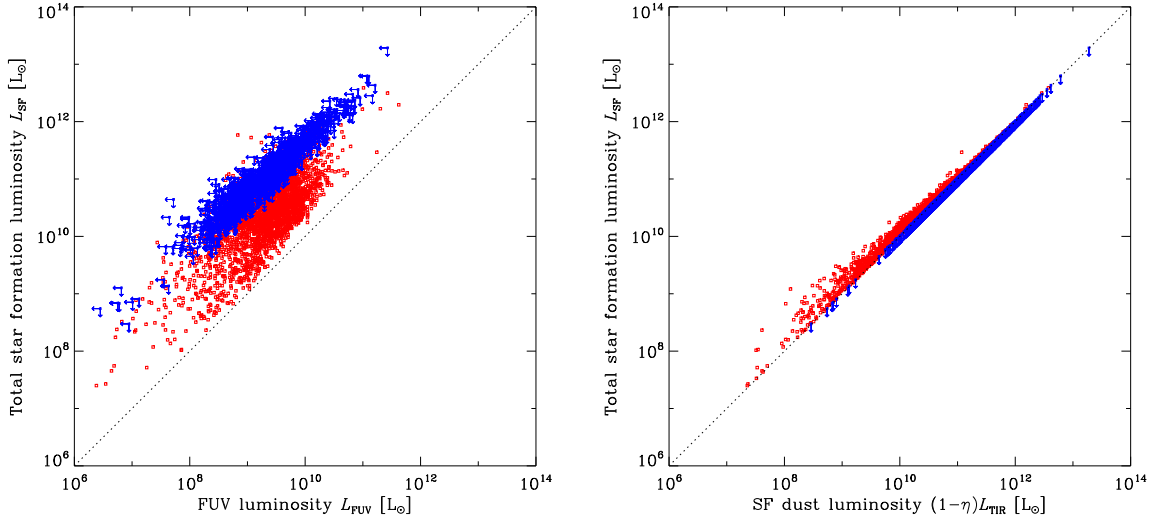


Fig. 6. Contributions of FUV and SF-related dust luminosities to SF luminosity. The left panel shows the contribution of FUV luminosity to the SF luminosity, and the right panel shows the contribution of the dust luminosity. Downward and left-pointing arrows represent galaxies which have UV flux densities below the detection limit of GALEX.

issue elsewhere (Takeuchi et al., 2012b).

3.4 Sample completeness

Now we examine the completeness of the final sample. From number counts of the sample, we expect that the flux limit is $S_{90} = 0.45$ Jy. The redshift completeness of the sample is tested by V/V_{\max} statistics (Schmidt 1968; Rowan-Robinson 1968). Here V is the volume enclosed in a sphere whose radius is the distance of a certain source in the sample, and V_{\max} is the volume enclosed in a sphere whose radius is the largest distance at which the source can be detected. If the sample is complete, V/V_{\max} of the sample galaxies is expected to be distributed uniformly between 0 and 1, with an average $\langle V/V_{\max} \rangle = 0.5$ and a standard deviation $(12)^{-1/2}$. For our final sample, we obtain $\langle V/V_{\max} \rangle = 0.51 \pm 0.27$, i.e., the sample can be regarded as complete down to 0.45 Jy. Thus, even if we have set additional conditions to have redshifts from IIFSCz, our sample is complete above this flux limit. The following analysis are all based on this limit.

3.5 Star formation luminosity

Now we compare FUV luminosity (mainly from massive stars) with TIR luminosity (mainly from dust) for the sample galaxies. Figure 5 shows that our sample galaxies are much more luminous at FIR than at FUV. Downward arrows in Fig. 5 represent galaxies which have UV flux densities below the detection limit of GALEX.

Here, we define the star formation luminosity, L_{SF} , as the total luminosity contributed only by massive stars. The SF luminosity is expressed as

$$L_{\text{SF}} \equiv L_{\text{FUV}} + (1 - \eta)L_{\text{TIR}}, \quad (11)$$

where η is the fraction of IR emission produced by dust heated by old stars, which is not related to the current SF. We adopted 30 % for this fraction (Hirashita et al., 2003) in the Local Universe. Buat et al. (2011) have shown that η is almost constant for a wide range of L_{TIR} for galaxies. Their result supports the assumption of a constant η .

Figure 6 shows the contributions of FUV and SF-related

dust luminosities to the SF luminosity. Here, the SF dust luminosity stands for $(1 - \eta)L_{\text{TIR}}$. The left panel in Fig. 6 shows the contribution of FUV luminosity to the SF luminosity, and the right panel shows the contribution of the SF dust luminosity. It is clearly seen that the galaxies are significantly above the diagonal line, and the scatter is large in the left panel. This comes directly from the fact that L_{TIR} is much larger than L_{FUV} . In contrast, the right panel of Fig. 6 shows a very tight correlation between $(1 - \eta)L_{\text{TIR}}$ and L_{SF} . We should note that, by definition, $(1 - \eta)L_{\text{TIR}} < L_{\text{SF}}$. However, as seen in Fig. 6, the galaxies with upper limits exactly delineate the diagonal line. For these galaxies, the SF activity is almost completely hidden by dust. We discuss this hidden SF in more detail in the next section.

4. Discussion

4.1 Star formation rate

Since we measure the emission from massive stars, we need to convert the number of massive stars to the total number of stars. We use an initial mass function (IMF) for this conversion. The IMF represents the number of newly formed stars per mass. We assume the Salpeter IMF (Salpeter, 1955).

With the spectral evolutionary synthesis model Starburst99 (Leitherer et al., 1999), and assuming a constant SFR over 10^8 yr, solar metallicity, and the Salpeter IMF (mass range $0.1M_{\odot}$ – $100M_{\odot}$), we obtain the relation between the SFR and L_{FUV} as (Iglesias-Páramo et al., 2006)

$$\log \text{SFR}_{\text{FUV}} = \log L_{\text{FUV}} - 9.51. \quad (12)$$

The relation between SFR and TIR luminosity is

$$\log \text{SFR}_{\text{dust}} = \log L_{\text{TIR}} - 9.75 + \log(1 - \eta), \quad (13)$$

where we have assumed that all stellar UV light is absorbed by dust. And we obtain the formula under the same assumption for both the star formation history (SFH) and the IMF as

those of the FUV. We obtain the following formula to calculate the total SFR:

$$\text{SFR} = \text{SFR}_{\text{FUV}} + \text{SFR}_{\text{dust}}, \quad (14)$$

where SFR_{FUV} is the SFR estimated from directly observable UV luminosity, and SFR_{dust} is that estimated from the dust luminosity.

The fraction of SFR_{FUV} to the total SFR for the sample galaxies is shown in Fig. 7. The scatter of the fraction is very large at $\text{SFR} < 20 \text{ M}_{\odot}\text{yr}^{-1}$. However, there is a sudden drop at $\text{SFR} > 20 \text{ M}_{\odot}\text{yr}^{-1}$. This means that the fraction of the hidden SF strongly depends on the SFR, and galaxies with higher SFRs are more strongly extinguished by dust.

We also find some outliers which have high SFRs and high SFR_{FUV} fractions. A possible explanation is that they might harbor quasars/AGNs. Since the UV energy of these objects is generated from accretion disks around central black holes, the efficiency of the energy release is much higher than for usual SF. As such, quasars tend to have a pointlike strong UV source in the center. In this case, L_{UV} is not related to the SF activity in a simple way so we do not discuss this further in this work. We cross matched the galaxies to the quasars/AGNs of Véron-Cetty & Véron (2010) and the identified galaxies are represented by the black crosses on the red or blue symbols in Fig. 7. We find that 246 objects in our sample are known quasars/AGNs. The ratio of quasars/AGNs to galaxies with $\text{SFR} \leq 20 \text{ M}_{\odot}\text{yr}^{-1}$ is 5.9% and the ratio of quasars/AGNs to galaxies with $\text{SFR} > 20 \text{ M}_{\odot}\text{yr}^{-1}$ is 11%. We also find that 6/9 galaxies which have $\text{SFR} > 20 \text{ M}_{\odot}\text{yr}^{-1}$ and $\text{SFR}_{\text{FUV}}/\text{SFR} > 0.3$ are quasars/AGNs. Thus, we can safely conclude that normal star-forming galaxies (without contamination of UV flux from AGNs) have small $\text{SFR}_{\text{FUV}}/\text{SFR}$ ratios. This is also consistent with the result by Totani et al. (2011) from a different aspect.

Figure 8 shows the ratio $\text{SFR}_{\text{FUV}}/\text{SFR}_{\text{dust}}$ as a function of L_{SF} . The similar ratio using SFR_{NUV} was presented in Iglesias-Páramo et al. (2006). We can relatively safely compare their result with ours, because SFR_{NUV} and SFR_{FUV} are calibrated from the same model, and the total IR luminosity in Iglesias-Páramo et al. (2006) is estimated with a formula proposed by Dale et al. (2001), which was proved to be a close approximation to our L_{TIR} (see Takeuchi et al., 2005b). We observe a larger scatter in Fig. 8 than Iglesias-Páramo et al. (2006). This may be because our sample is much larger and contains more extremely dusty objects.

Figure 9 shows the relation between SFR and L_{TIR} . We find a very tight correlation. Comparing our result with the result of Bothwell et al. (2011), there are more galaxies in the regime with higher L_{TIR} ($L_{\text{TIR}} \gtrsim 10^{12} L_{\odot}$) and higher SFR ($\text{SFR} \gtrsim 10^2 \text{ M}_{\odot}\text{yr}^{-1}$), and few galaxies in the lower L_{TIR} ($L_{\text{TIR}} \lesssim 10^8 L_{\odot}$) and lower SFR ($\text{SFR} \lesssim 10^{-1} \text{ M}_{\odot}\text{yr}^{-1}$) regime. This is because Bothwell et al. (2011) added low-luminosity local volume galaxies to their IR- and UV-selected samples, and they made a volume correction on these data, while our sample is only IR-selected.

We also see that galaxies with FUV flux densities below the GALEX detection limit delineate the same trend which was reported by Bothwell et al. (2011). Further, galaxies with $\text{SFR} < 10^{-1} \text{ M}_{\odot} \text{yr}^{-1}$ start to deviate from the general

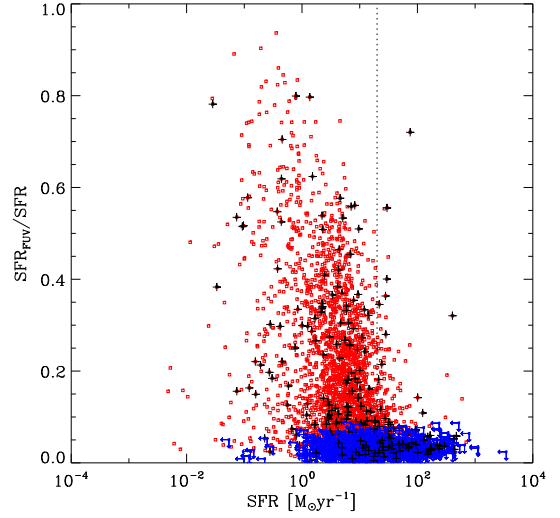


Fig. 7. Contribution of the fraction of SFR_{FUV} to the total SFR. The red and blue symbols are the same as in Fig. 6. The black crosses represent the quasars and active galaxies cross matched to the objects by Véron-Cetty & Véron (2010). The dotted line represents the total SFR where $\text{SFR}_{\text{FUV}}/\text{SFR}$ drops suddenly for increasing SFR.

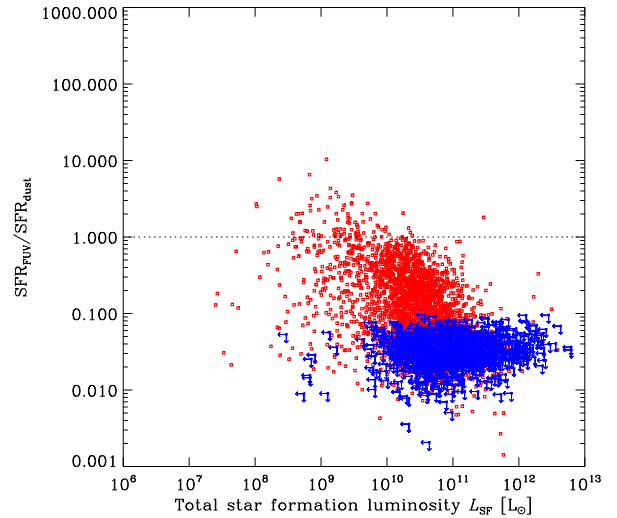


Fig. 8. Ratio between SFR_{FUV} and SFR_{TIR} as a function of star-formation luminosity L_{SF} . The red and blue symbols are the same as in Fig. 6.

trend, also consistent with Bothwell et al. (2011). This confirms that galaxies with low SFR have larger contributions from SFR_{FUV} .

4.2 Dust extinction

The relation between L_{SF} and the infrared excess $\text{IRX} \equiv L_{\text{TIR}}/L_{\text{FUV}}$, known as an indicator of extinction as a function of IR luminosities, is shown in Fig. 10. Figure 10 has the trend that galaxies which have larger L_{SF} have high IRX, consistent with Fig. 7 of Buat et al. (2007).

Rather naturally, we expected strong dust extinction for the current sample because they are IR-selected. We find a similar result to that of Buat et al. (2005) and Takeuchi et al. (2010).

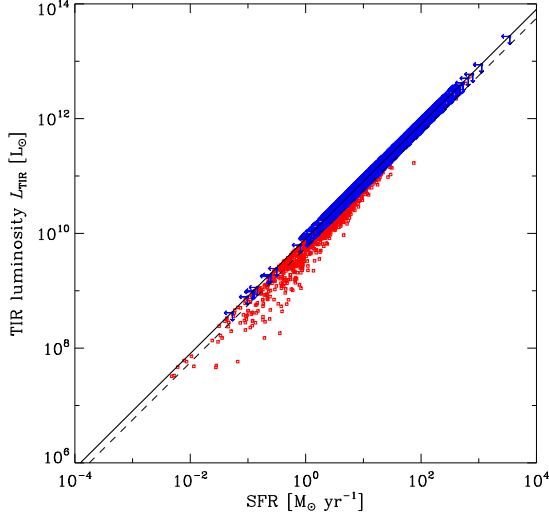


Fig. 9. Relation between SFR and L_{TIR} . The red and blue symbols are the same as in Fig. 6. The solid line represents the L_{TIR} -SFR scaling given by Eq. (13). The dotted line represents the L_{FIR} -SFR scaling given by Iglesias-Páramo et al. (2006).

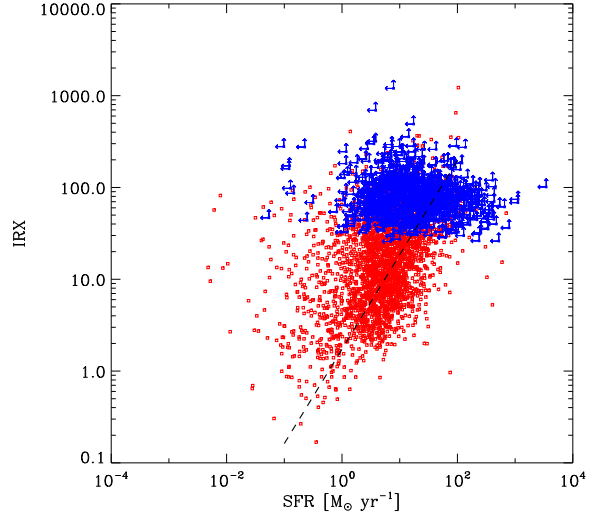


Fig. 11. Relation between SFR and IRX. The red and blue symbols are the same as in Fig. 10. The dotted line represents the IRX-SFR relation derived for star-forming $z \sim 0$ galaxies by Overzier et al. (2011).

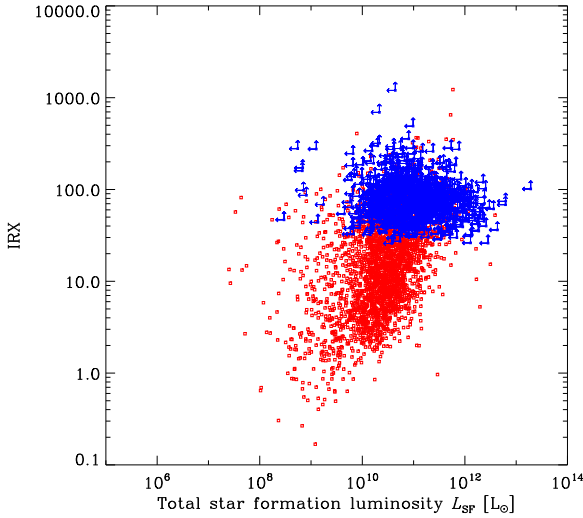


Fig. 10. Relation between L_{SF} and the infrared excess $\text{IRX} \equiv L_{\text{TIR}}/L_{\text{FUV}}$. Upward and left-pointing arrows represent galaxies which have UV flux densities below the detection limit of GALEX. The scatter of the IRX is large.

Figure 11 shows the relation between SFR and IRX. Again, we compare it with Fig. 10 of Bothwell et al. (2011). Since we plot the sample galaxies directly without a volume correction, it is not straightforward to compare the distribution of galaxies on this figure. Even so, we can see that we have less galaxies in the low SFR ($\text{SFR} < 10^{-1} \text{ M}_{\odot} \text{ yr}^{-1}$) and small attenuation ($\text{IRX} < 1$) regime compared with Bothwell et al. (2011). As for Fig. 9, this comes from the effects of sample selection and our sample is inclined to more luminous galaxies because of the IR-selection. The global trend is, however, almost the same for Bothwell et al. (2011).

Figure 12 shows the relation between the FUV-NUV color and IRX. The galaxies which have UV flux densities

below the detection limit are not plotted. We show the dependence on the two different IR luminosities, $L_{\text{IRAS}60\mu\text{m}}$ and L_{TIR} , for comparison with various previous studies. In general, L_{TIR} is smaller than $L_{\text{IRAS}60\mu\text{m}}$ as you can also see in Fig. 9. We can compare the left panel of Fig. 12 with Fig. 15 of Takeuchi et al. (2010) directly, and find a similar trend. By contrast, L_{TIR} is more directly connected to the definition of IR luminous galaxies, LIRGs ($10^{11} L_{\odot} \leq L_{\text{TIR}} < 10^{12} L_{\odot}$) and ultra IR luminous galaxies, ULIRGs ($10^{12} L_{\odot} \leq L_{\text{TIR}}$). Indeed, more galaxies in the right panel are identified as the IR luminous galaxies according to the criterion of L_{TIR} dependence. Solid curves in each panel represent the revised $\text{IRX}-\beta$ relation obtained from the GALEX-AKARI measurement of the same UV-luminous starbursts as Meurer et al. (1999), proposed by Takeuchi et al. (2012a). Most IR luminous galaxies are above the curve in each panel. This trend was discovered by Goldader et al. (2002) and followed by subsequent studies (e.g., Buat et al., 2005; Takeuchi et al., 2010, among others). On the other hand, non IR luminous galaxies, i.e. lower extinction galaxies, follow this curve. This may be explained as follows: Takeuchi et al. (2012a) used the same original galaxy sample of Meurer et al. (1999), which was selected for central UV-luminous intense starbursts. Since these galaxies tend to have lower dust attenuation than LIRGs/ULIRGs, they are similar to the lower-IR luminosity galaxies in our sample having significant UV fluxes, as we have seen in Fig. 9. Hence, we conclude that low-luminosity IR galaxies have a common attenuation strength with UV-luminous starbursts.

5. Conclusions

We analyzed star formation-related properties of Local galaxies using AKARI and GALEX data. The summary and conclusions of this study are as follows:

- 1) The star formation luminosity, L_{SF} , is dominated by the emission from dust related to SF activity, $(1 - \eta)L_{\text{TIR}}$.

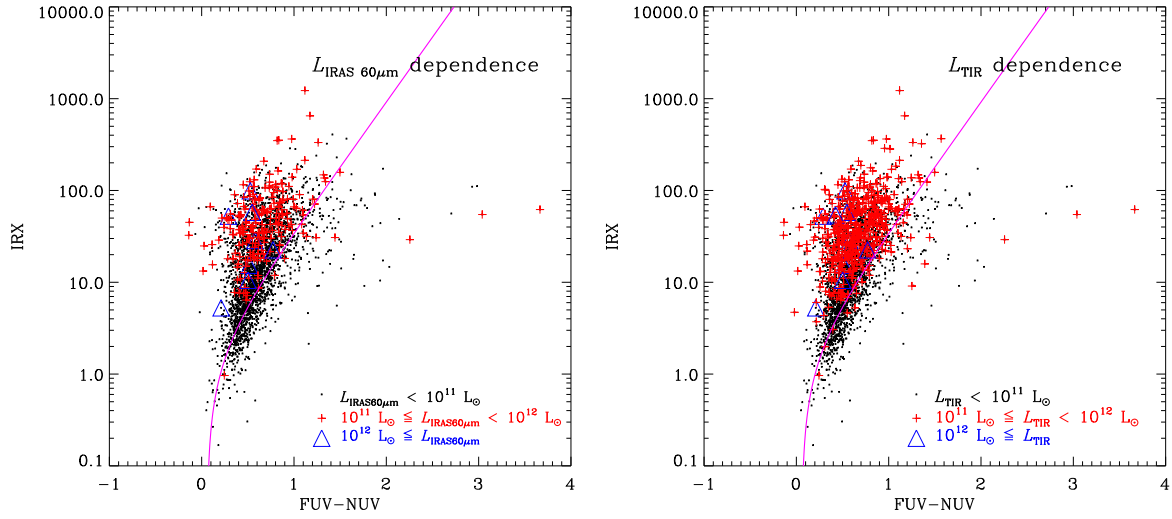


Fig. 12. Relation between FUV–NUV color and IRX. The left panel shows the relation as a function of IRAS 60 μ m luminosity, $L_{\text{IRAS } 60\mu\text{m}}$. The right panel is the same but with total IR luminosity, L_{TIR} . Dots: galaxies with $L_{\text{IR}} < 10^{11} L_{\odot}$, crosses: galaxies with $10^{11} L_{\odot} \leq L_{\text{IR}} < 10^{12} L_{\odot}$, triangles: galaxies with $L_{\text{IR}} \leq 10^{12} L_{\odot}$. Here L_{IR} stands for $L_{\text{IRAS } 60\mu\text{m}}$ in the left panel and L_{TIR} in the right panel. The solid curve in each panel represents the IRX–UV-color relation of UV-luminous starbursts (Takeuchi et al., 2012a).

- 2) The contribution of ultraviolet luminosity, L_{FUV} , has a larger scatter than that of the contribution of $(1 - \eta)L_{\text{TIR}}$.
- 3) It is difficult to estimate the star formation activity only from the relation between L_{SF} and L_{FUV} because of the small contribution of L_{FUV} .
- 4) Galaxies with higher SF activity ($\text{SFR} > 20 M_{\odot} \text{ yr}^{-1}$) have a higher fraction of their SF hidden by dust.
- 5) We examined the relation between IRX, $L_{\text{TIR}}/L_{\text{FUV}}$, and FUV–NUV color. Among the current sample, low-IR luminosity galaxies ($< 10^{11} L_{\odot}$) follow the relation for UV-luminous starbursts proposed by Takeuchi et al. (2012a).

These conclusions are consistent with those of Takeuchi et al. (2010). However, we find that the dispersion in various relations they obtained suffered from the noise of the AKARI BSC β -1 catalog. In this study, the S/N is three times better so we do not share the same problem. Thus, we can safely conclude that the above properties are general features of Local star-forming dusty galaxies.

Acknowledgments. This work is based on observations with AKARI, a JAXA project with the participation of ESA. TTT has been supported by Program for Improvement of Research Environment for Young Researchers from Special Coordination Funds for Promoting Science and Technology, and the Grant-in-Aid for the Scientific Research Fund (20740105, 23340046, 24111707) commissioned by the MEXT. AS, TTT, and FTY have been partially supported from the Grand-in-Aid for the Global COE Program “Quest for Fundamental Principles in the Universe: from Particles to the Solar System and the Cosmos” from the Ministry of Education, Culture, Sports, Science and Technology (MEXT) of Japan. We are grateful to Stefan Noll and the anonymous referee for their helpful comments which improved the presentation and content of this paper. We deeply thank Noriko Tsuchiya for her early contribution to this work, and Jennifer M. Stone and Aleksandra Solarz for their help in the improvement of English.

References

- Asano, R. S., Takeuchi, T. T., Hirashita, H., Inoue, A. K., Dust formation history of galaxies: a critical role of metallicity for the dust mass growth by accreting materials in the interstellar medium, *Earth, Planets, & Space*, in press (astro-ph/1206.0817), 2012.
- Bothwell, M. S., Kenicutt, R. C., Johnson, B. D., Wu, Y., Lee, J. C., Dale, D., Engelbracht, C., Calzetti, D., Skillman, E., The star formation rate distribution function of the local Universe, *Monthly Notices of the Royal Astronomical Society*, **415**, 1815–1826, 2011.
- Buat, V., Burgarella, D., The observation of the nearby universe in UV and in FIR: an evidence for a moderate extinction in present day star forming galaxies, *Astronomy and Astrophysics*, **334**, 772–782, 1998.
- Buat, V., et al. Dust Attenuation in the Nearby Universe: A Comparison between Galaxies Selected in the Ultraviolet and in the Far-Infrared, *The Astrophysical Journal*, **619**, L51–L54, 2005.
- Buat, V., Takeuchi, T. T., Iglesias-Páramo, J., et al., The Local Universe as Seen in the Far-Infrared and Far-Ultraviolet: A Global Point of View of the Local Recent Star Formation, *The Astrophysical Journal Supplement Series*, **469**, 19–25, 2007.
- Buat, V. and Giovannoli, E. and Takeuchi, T. T. and Heinis, S. and Yuan, F.-T. and Burgarella, D. and Noll, S. and Iglesias-Páramo, J., Spectral energy distributions of an AKARI-SDSS-GALEX sample of galaxies, *Astronomy and Astrophysics*, **529**, A22, 2011.
- Calzetti, D., et al., The Calibration of Monochromatic Far-Infrared Star Formation Rate Indicators, *The Astrophysical Journal*, **714**, 1256–1279, 2010.
- Cardelli, J. A., Clayton, G. C., & Mathis, J. S., The relationship between infrared, optical, and ultraviolet extinction, *Astronomy and Astrophysics*, **345**, 245–256, 1989.
- Cortese, L., Boselli, A., Buat, V., Gavazzi, G., Boissier, S., Gil de Paz, A., Seibert, M., Madore, B. F., Martin, D. C., UV Dust Attenuation in Normal Star-Forming Galaxies. I. Estimating the $L_{\text{TIR}}/L_{\text{FUV}}$ Ratio, *The Astrophysical Journal*, **637**, 242–254, 2006.
- Cucciati, O., et al. The star formation rate density and dust attenuation evolution over 12 Gyr with the VVDS surveys, *Astronomy and Astrophysics*, **539**, A31, 2012.
- Dale, D. A., Helou, G., Contursi, A., Silberman, N. A., Kolhatkar, S., The Infrared Spectral Energy Distribution of Normal Star-forming Galaxies, *The Astrophysical Journal*, **549**, 215–227, 2001.
- Goldader, J. D., Meurer, G., Heckman, T. M., Seibert, M., Sanders, D. B., Calzetti, D., Steidel, C. C. 2002. Far-Infrared Galaxies in the Far-Ultraviolet. *The Astrophysical Journal* 568, 651–678.
- Haines, C. P., Busarello, G., Merluzzi, P., Smith, R. J., Raychaudhury, S., Mercurio, A., Smith, G. P., ACCESS - II. A complete census of star formation in the Shapley supercluster - UV and IR luminosity functions,

- Monthly Notices of the Royal Astronomical Society*, **412**, 127–144, 2011.
- Hao, C.-N., Kennicutt, R. C., Johnson, B. D., Calzetti, D., Dale, D. A., Moustakas, J. Dust-corrected Star Formation Rates of Galaxies. II. Combinations of Ultraviolet and Infrared Tracers, *The Astrophysical Journal*, **741**, 124, 2011.
- Hirashita, H., Buat, V., & Inoue, A. K., Star formation rate in galaxies from UV, IR, and H α estimators, *Astronomy and Astrophysics*, **410**, 83–100, 2003.
- Hirashita, H., Kaneda, H., Onaka, T., Suzuki, T., Far-Infrared Properties of Blue Compact Dwarf Galaxies Observed with AKARI/Far-Infrared Surveyor (FIS), *Publications of the Astronomical Society of Japan*, **60**, S477–488, 2008.
- Iglesias-Páramo, J., et al., Star Formation in the Nearby Universe: The Ultraviolet and Infrared Points of View, *The Astrophysical Journal Supplement Series*, **164**, 38–51, 2006.
- Kawada, M., et al., The Far-Infrared Surveyor (FIS) for AKARI, *Publications of the Astronomical Society of Japan*, **59**, 389–400, 2007.
- Kawada, M., et al., Performance of an Imaging Fourier Transform Spectrometer with Photoconductive Detector Arrays: An Application for the AKARI Far-Infrared Instrument, *Publications of the Astronomical Society of Japan*, **60**, S389–397, 2008.
- Kennicutt, R. C., Jr., Star Formation in Galaxies Along the Hubble Sequence, *Annual Review of Astronomy and Astrophysics*, **36**, 189–232, 1998.
- Kennicutt, R. C., Jr., Hao, C.-N., Calzetti, D., et al., Dust-corrected Star Formation Rates of Galaxies. I. Combinations of H α and Infrared Tracers, *The Astrophysical Journal*, **703**, 1672–1695, 2009.
- Lee, J. C., et al., Comparison of H α and UV Star Formation Rates in the Local Volume: Systematic Discrepancies for Dwarf Galaxies, *The Astrophysical Journal*, **706**, 599–613, 2009.
- Leitherer, C., Schaerer, D., Goldader, J. D., et al., Starburst99: Synthesis Models for Galaxies with Active Star Formation, *The Astrophysical Journal Supplement Series*, **123**, 3–40, 1999.
- Martin, D. C., et al., The Star Formation Rate Function of the Local Universe, *The Astrophysical Journal*, **619**, L59–L62, 2005.
- Mathis, J. S., Interstellar dust and extinction, *ARA&A*, **28**, 37–70, 1990.
- Meurer, G. R., Heckman, T. M., & Calzetti, D. Dust Absorption and the Ultraviolet Luminosity Density at $z \approx 3$ as Calibrated by Local Starburst Galaxies, *The Astrophysical Journal*, **521**, L64–L80, 1999.
- Morrissey, P., et al., The Calibration and Data Products of GALEX, *Astronomy and Astrophysics*, **173**, 682–697, 2007.
- Murakami, H., et al., The Infrared Astronomical Mission AKARI, *Publications of the Astronomical Society of Japan*, **59**, S369–376, 2007.
- Murphy, E. J., Chary, R.-R., Dickinson, M., Pope, A., Frayer, D. T., An Accounting of the Dust-obscured Star Formation and Accretion Histories Over the Last ~ 11 Billion Years, *The Astrophysical Journal*, **732**, 126, 2011.
- Noll, S., Burgarella, D., Giovannoli, E., Buat, V., Marcellac, D., Muñoz-Mateos, J. C., Analysis of galaxy spectral energy distributions from far-UV to far-IR with CIGALE: studying a SINGS test sample, *Astronomy and Astrophysics*, **507**, 1793–1813, 2009.
- Onaka, T., et al., The Infrared Camera (IRC) for AKARI – Design and Imaging Performance, *Publications of the Astronomical Society of Japan*, **59**, 401–410, 2007.
- Overzier, R. A., Heckman, T. M., Wang, J., Dust Attenuation in UV-selected Starbursts at High Redshift and Their Local Counterparts: Implications for the Cosmic Star Formation Rate Density, *The Astrophysical Journal Letters*, **726**, L7, 2011.
- Pollo, A., Rybka, P., & Takeuchi, T. T., Star-galaxy separation by far-infrared color-color diagrams for the AKARI FIS all-sky survey (bright source catalog version β -1), *Astronomy and Astrophysics*, **514**, A3, 2010.
- Rowan-Robinson, M., The determination of the evolutionary properties of quasars by means of the luminosity-volume test, *Monthly Notices of the Royal Astronomical Society*, **138**, 445, 1968.
- Salpeter, E. E., The Luminosity Function and Stellar Evolution., *The Astrophysical Journal*, **121**, 161, 1955.
- Sanders, D. B., & Mirabel, I. F., Luminous Infrared Galaxies, *Astronomy and Astrophysics*, **34**, 749–792, 1996.
- Schlegel, D. J., Finkbeiner, D. P., & Davis, M., Maps of Dust Infrared Emission for Use in Estimation of Reddening and Cosmic Microwave Background Radiation Foregrounds, *Astronomy and Astrophysics*, **500**, 525–553, 1998.
- Schmidt, M., Space Distribution and Luminosity Functions of Quasi-Stellar Radio Sources, *The Astrophysical Journal*, **151**, 393, 1968.
- Seibert, M., et al., Testing the Empirical Relation between Ultraviolet Color and Attenuation of Galaxies, *The Astrophysical Journal*, **619**, L55–L58, 2005.
- Soifer, B. T., Neugebauer, G., & Houck, J. R., The IRAS view of the extragalactic sky, *Annual Review of Astronomy and Astrophysics*, **25**, 187–230, 1987.
- Takeuchi, T. T., Buat, V., Burgarella, D. The evolution of the ultraviolet and infrared luminosity densities in the universe at $0 < z < 1$, *Astronomy and Astrophysics*, **440**, L17–L20, 2005.
- Takeuchi, T. T., Buat, V., Iglesias-Páramo, J., Boselli, A., & Burgarella, D., Mid-infrared luminosity as an indicator of the total infrared luminosity of galaxies, *Astronomy and Astrophysics*, **432**, 423–429, 2005.
- Takeuchi, T. T., Buat, V., Heinis, S., Giovannoli, E., Yuan, F.-T., Iglesias-Páramo, J., Murata, K. L., & Burgarella, D., Star formation and dust extinction properties of local galaxies from the AKARI-GALEX all-sky surveys. First results from the most secure multiband sample from the far-ultraviolet to the far-infrared, *Astronomy and Astrophysics*, **514**, A4, 2010.
- Takeuchi, T. T., Sakurai, A., Yuan, F.-T., Buat, V., Burgarella, D., Far-Ultraviolet and Far-Infrared Bivariate Luminosity Function of Galaxies: Complex Relation between Stellar and Dust Emission, *Earth, Planets, & Space*, in press (astro-ph/1206.5950), 2012.
- Takeuchi, T. T., Yuan, F.-T., Ikeyama, A., Murata, K. L., & Inoue, A. K., Reexamination of the Infrared Excess-Ultraviolet Slope Relation of Local Galaxies, *The Astrophysical Journal*, in press (astro-ph/1206.3905), 2012.
- Totani, T., Takeuchi, T. T., Nagashima, M., Kobayashi, M. A. R., Makiya, R. Infrared Spectral Energy Distribution of Galaxies in the AKARI All Sky Survey: Correlations with Galaxy Properties, and Their Physical Origin, *Publications of the Astronomical Society of Japan*, **63**, 1181–1206, 2011.
- Véron-Cetty, M.-P. and Véron, P., A catalogue of quasars and active nuclei: 13th edition, *Astronomy and Astrophysics*, **518**, A10, 2010.
- Wang, L., Rowan-Robinson, M., The Imperial IRAS-FSC Redshift Catalogue, *Monthly Notices of the Royal Astronomical Society*, **398**, 109–118, 2009.
- Yamamura, I., Fukuda, Y., & Makiuti, S., AKARI/FIS All-Sky Survey Bright Source Catalogue Version β -1 Release Note (Rev. 1), ISAS/JAXA, 2008.
- Yamamura I., Makiuti S., Ikeda N., Fukuda Y., Oyabu S., Koga T., White G. J., AKARI/FIS All-Sky Survey Bright Source Catalogue Version 1.0 Release Note, ISAS/JAXA, 2010.

A. Sakurai (e-mail: sakurai.akane@e.mbox.nagoya-u.ac.jp)